Wind and Structures, *Vol. 25, No. 2 (2017) 195-214*
DOI: https://doi.org/10.12989/was.2017.25.2.195

Wind characteristics at Sutong Bridge site using 8-year field measurement data

Xu Zidong[1], Wang Hao[*1], Wu Teng[2], Tao Tianyou[1] and Mao Jianxiao[1]

[1]*Key Laboratory of Concrete and Prestressed Concrete Structure of the Ministry of Education, Southeast University, Nanjing 210096, China*
[2]*Department of Civil, Structural and Environmental Engineering, University at Buffalo, The State University of New York, Buffalo, NY 14260, USA*

(Received October 20, 2016, Revised July 8, 2017, Accepted July 10, 2017)

Abstract. Full-scale wind characteristics based on the field measurements is an essential element in structural wind engineering. Statistical analysis of the wind characteristics at Sutong Cable-stayed Bridge (SCB) site is conducted in this study with the recorded long-term wind data from structural health monitoring system (SHMS) between 2008 and 2015. Both the mean and turbulent wind characteristics and power spectra are comprehensively investigated and compared with those in the current codes of practice, such as the measured wind rose diagram, monthly maximum mean wind speed, turbulence intensity, integral length scale. Measurement results based on the monitoring data show that winds surrounding the SCB site are substantially influenced by the southeast monsoon in summer and strong northern wind in winter. The measured turbulence intensity is slightly higher than the recommended values in specifications, while the measured ratio of lateral to longitudinal turbulence intensity is slightly lower. An approximately linear relationship between the measured turbulence intensities and gust factors is obtained. The mean value of the turbulence integral length scale is smaller than that of typical typhoon events. In addition, it is found that the Kaimal spectrum is suitable to be adopted as the power spectrum for longitudinal wind component at the SCB site. This contribution would provide important wind characteristic references for the wind performance evaluation of SCB and other civil infrastructures in adjacent regions.

Keywords: wind characteristics; turbulence; long-term monitoring; Sutong Bridge; structural health monitoring system

1. Introduction

A number of long-span cable-supported bridges have been built all over the world, particularly in China during the past two decades, which has significantly advanced the design and construction methodologies. These long-span bridges are commonly constructed to cross the straights or deep-cutting valleys, hence are vulnerable to strong winds and typhoons. Typically, the wind-structure interaction is a governing factor during the design, construction and operational stages of long-span cable-supported bridges. Full-scale wind characteristics based on the field measurements is essential to accurately modeling wind effects on structures (e.g., Huang *et al.*

*Corresponding author, Professor, E-mail: wanghao1980@seu.edu.cn

http://www.techno-press.org/?journal=was&subpage=8 ISSN: 1226-6116 (Print), 1598-6225 (Online)

2015, Wang *et al.* 2016). Several databases of wind characteristics have been well established (e.g., Andersen and Lovseth 1995, Wills *et al.* 1986, Sparks *et al*. 1992), which facilitates the wind climate research. However, most of the wind databases are not necessarily applicable to the structural wind engineering.

Researches of wind characteristics based on the field measurements with a concern of their effects on civil infrastructures have also been carried out in history. For example, Deaves and Harris (1978) concluded that, with the full-scale wind data in Cardington, the turbulence intensity, power spectra and wind profile apparently vary according to turbulence integral length and altitude, while turbulence integral length is related to surface roughness. Sharma and Richards (1999) found that the improved turbulence level of typhoon is related to convective stability and the non-stationary wind spectra. Toriumi *et al.* (2000) analyzed the spatial correlation of the longitudinal turbulence with field-measurement data for Akashi Kaikyo Bridge and Darmngmen Bridge during the typhoon. Recently, Li *et al.* (2012) proposed a data-driven model for wind spectra in tropical cyclone winds over the sea surface. Xiao *et al.* (2010) and Li *et al*. (2015) analyzed the difference of wind characteristics between typhoon and hurricane. However, most of the aforementioned field measurements are based on the data from the meteorological station with lower sampling frequency than those of the anemometers of SHMS, and hence is not suitable for the analysis of wind characteristics. The long-term field measurement of wind characteristics based on the structural health monitoring systems (SHMSs) is of great significance for engineers to take full advantage of realistic wind environment at structural sites (Miyata *et al*. 2002, Zhang *et al*. 2010). Although measurements from SHMSs have been employed particularly in China to promote the structural wind engineering in China (Hui *et al*. 2009, Li *et al*. 2009, Wang *et al*. 2013), statistical analysis of wind characteristics using long-term field data measured from structures is still insufficient. Such databases based on SHMS could also be employed to advance the theoretical analysis of the wind-induced vibrations of wind-sensitive structures (Xu *et al*. 2000, Fu *et al*. 2008), and hence there's a need for more to be collected and expanded with appropriate statistical treatments.

In this study, the recorded long-term real-time wind data from Jan. 2008 to Mar. 2015 are utilized to analyze the wind characteristics at the SCB site, including the mean wind speed, turbulence intensity, gust factor, turbulence integral length and the turbulence power spectral density. Comparative analyses between results from the field-measurement data and values in the codes of practice are conducted. The findings would provide important wind characteristic references for not only maintenance management and wind-performance evaluation of the SCB site, but also other civil infrastructures in adjacent regions.

2. Description of SCB

2.1 Wind climate at SCB location

The SCB, across the Yangtze River in Jiangsu Province, China, was opened to traffic in May 2008 (You *et al.* 2008). The main span of the cable stayed bridge is 1088 m, as shown in Fig. 1.

The bridge axis is with a clockwise 10.6 degree to the due north direction. The meteorology survey reveals that the SCB site is dominated by the southern subtropical humid monsoon climate.

The seasonal changes of the local wind environment at the SCB site is caused by the monsoon circulation. The typhoons in summer and strong northern wind in winter are primary wind loads of the bridge The structural wind-resistant design with reliable wind characteristics is therefore imperative to this long-span flexible structure.

2.2 The layout of anemometers

SHMS provides opportunities to observe more realistic structure behaviors under operational excitations and further evaluate structural safety status (Deng *et al.* 2015). 15 types of sensors have been installed on SCB for real-time monitoring of structural responses, geometric deformations, environmental conditions, and traffic loads by using modern techniques in sensing, testing, and network communications.

As shown in Fig. 1, four anemometers, namely FS4, FS4’, FS2 and FS6, are equipped in order to study the wind characteristics at the bridge site. The anemometers FS4 and FS4’ are installed in the middle of the main span with an elevation of 76m. More specifically, the FS4 anemometer is installed on the upstream side while the FS4’ anemometer is on the downstream side. To reduce the screening effect by the bridge structure, the anemometers FS4 and FS4’ are installed 4.0 m higher than the deck via stable supports. As there are two anemometers at the mid-span, the differences between the turbulence intensities could tell the direction of the incoming wind since the downstream wind could be interfered by the bridge deck and therefore contains more turbulence. Meanwhile, the anemometers FS6 and FS2 (306 m high), respectively, are installed at the top of the south and north towers to monitor the wind environment at the top of the structure. The effectiveness of the recorded real-time wind data in strong typhoons verifies the reliability of this system (Wang *et al.* 2013).

3. Mean wind characteristics at SCB site

In this study, a 10-min duration is selected as a basic interval during the analysis. Based on the vector decomposition method, the mean wind speed U and mean wind direction Φ in the cartesian coordinate system can be conveniently obtained (Li *et al.* 2009, Pang *et al.* 2002). The wind direction is defined as 0° facing north, and the clockwise rotation is set to be positive. To avoid vast amounts of data, a sampling frequency of 1 Hz is sufficient and thus adopted for the real-time monitoring.

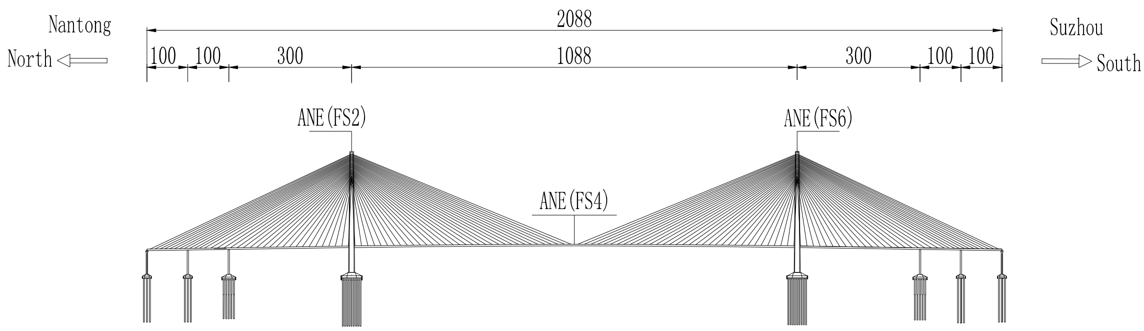

Fig. 1 Layout of Anemometers on SCB (Unit: m)

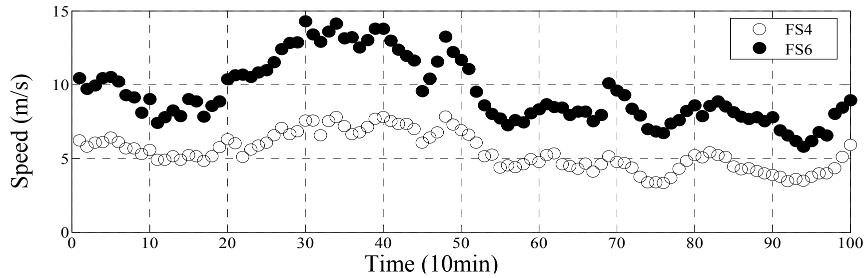

(a) 10-min mean wind speed (normal wind data segment)

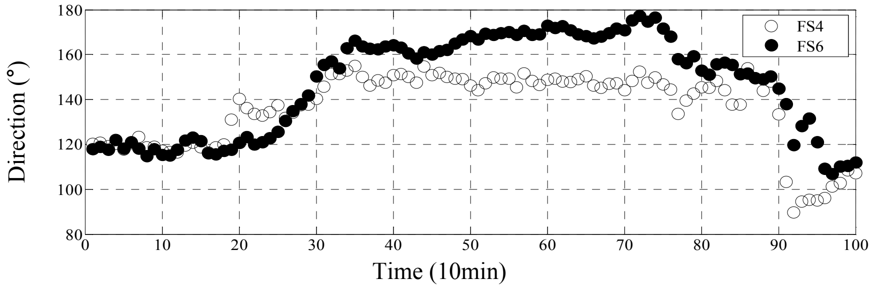

(b) 10-min mean wind direction (normal wind data segment)

Fig. 2 Averaged wind data on bridge deck and top of the tower under normal conditions

3.1 Measured data at various altitudes

The measured data from 12:00 on Apr. 18 to 4:00 on Apr. 19, 2010 and data from 14:00 on Aug. 3 to 06:00 on Aug. 4, 2012 (Typhoon Damrey) by FS4 and FS6 are selected respectively to investigate the relationship of the wind characteristics at different altitudes for various wind scenarios. Figs. 2 and 3, respectively, show the variation trend of the averaged wind data in a 10-min interval measured from bridge deck and the top of the tower. The two sets of monitored data from SHMS present similar fluctuation for various wind scenarios, which validates the reliability of the data.

Since the wind loads under typical strong winds on the bridge deck is most important to be considered compared to other components, data measured by FS4 from Jan. 1, 2008 to Mar. 31, 2015 are selected for analysis in this study. Fig. 4 just presents the wind data of the time segment from June, 2010 to December, 2010 for better illustration.

3.2 Wind rose diagram at SCB site

Wind rose diagram, as a professional statistical chart, reflects the occurrence frequency of wind in sixteen statistical directions. It could be calculated by

$$P_n = \frac{f_n}{\sum_{1}^{16} f_n} \tag{1}$$

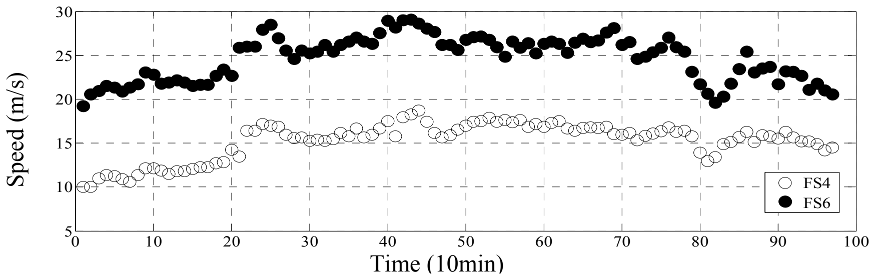

(a) 110-min mean wind speed (Typhoon Damrey data segment)

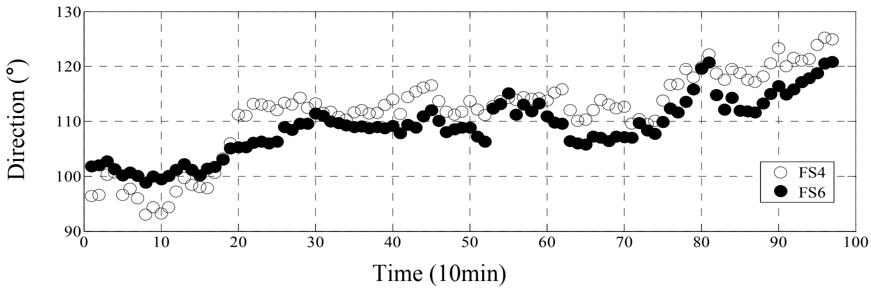

(b) 10-min mean wind direction (Typhoon Damrey data segment)

Fig. 3 Averaged wind data on bridge deck and top of the tower during Typhoon Damrey

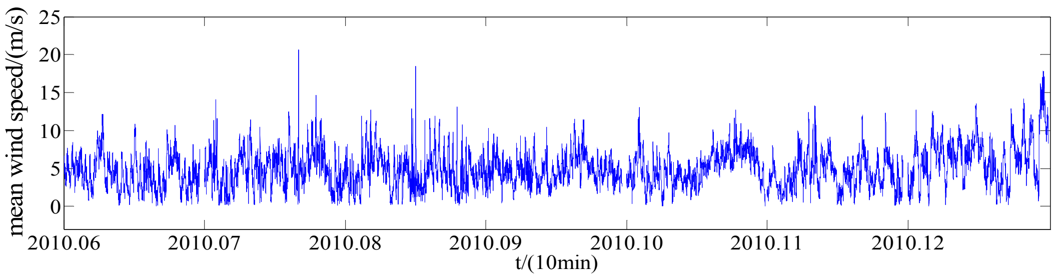

Fig. 4 10-min mean wind speed of a typical normal wind condition on the center of bridge deck

where P_n is the wind frequency in the nth direction, with the azimuth angle range of 22.5°; f_n is the occurrence frequency of wind in the nth direction.

Fig. 5 shows the long-term mean wind characteristics, i.e., the rose diagram of wind direction, average wind speed and maximum wind speed, based on the measured data at SCB site. Fig. 5(a) indicates the dominance of southeast wind at SCB site, with an occurrence frequency of around 12%. Fig. 5(b) demonstrates the mean wind speed ranging from 4.1 to 6.7 m/s fluctuates slightly in various directions. The maximum mean wind speed in southeast direction is larger than 20 m/s as shown in Fig. 5(c), which coincides with the climate condition at SCB site. The mean wind speed in north direction is less than 5 m/s while the maximum wind speed is larger than 15 m/s, which is closely related to the strong northern wind from Siberia.

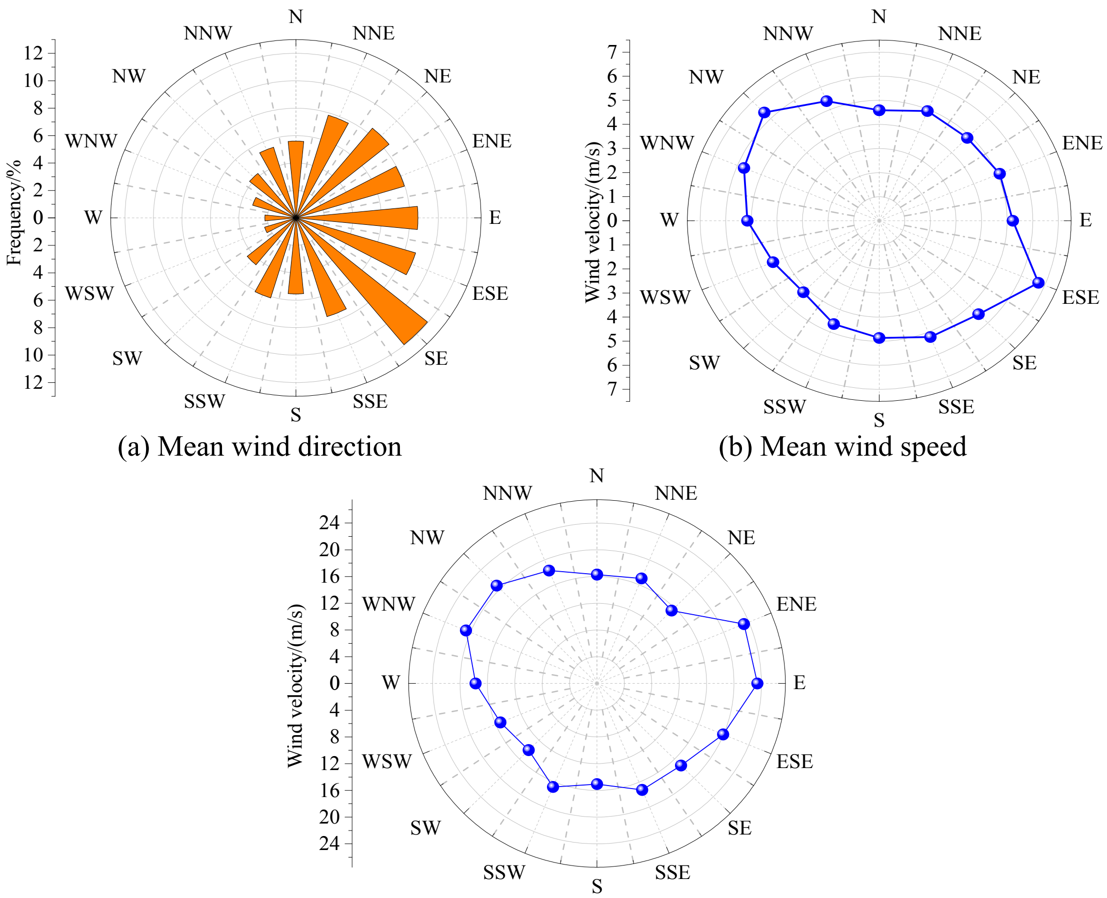

(a) Mean wind direction (b) Mean wind speed

(c) Maximum mean wind speed

Fig. 5 Rose diagram at SCB site

3.3 Monthly maximum wind speed at SCB site

In order to further investigate the wind speed for various months, the monthly maximum wind speeds are analyzed, as shown in Fig. 6.

Fig. 6 reflects a rising trend of monthly maximum wind speed from January to April, while the overall trend of monthly extreme wind speed remains approximately constant at a higher level from June to August. The extreme wind speed in winter is also relatively large due to the effects of strong northern winds. To sum up, apparent correlation exists between the extreme wind speed and seasonal climate effects, which further verifies the reliability of the measured data based on the SHMS of SCB.

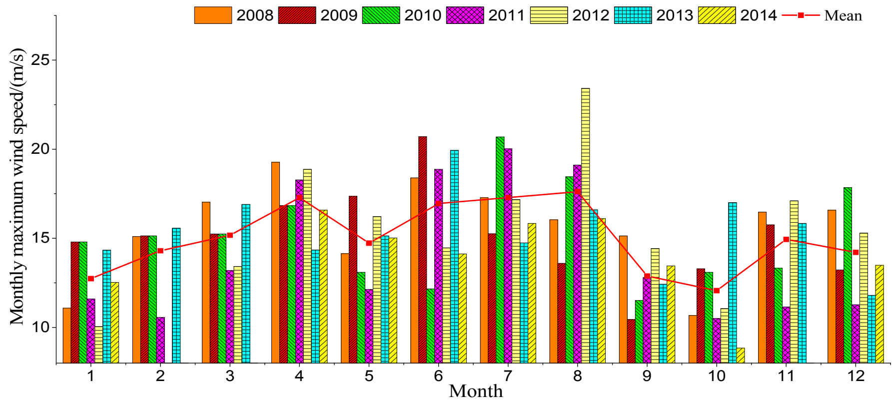

Fig. 6 Variation of monthly maximum wind speed

4 Turbulent wind characteristics at SCB site

4.1 Turbulence intensity

Turbulence intensity is defined as the ratio of the mean square deviation of turbulent wind speed to the mean wind speed

$$I_u = \frac{\sigma_u}{U}, I_v = \frac{\sigma_v}{U} \tag{2}$$

where σ_u and σ_v respectively represent the longitudinal and lateral mean square deviation of turbulent wind speed. Since there is limited meaning of very low-speed wind data for the structural responses under winds, only the wind data with mean wind speed larger than 6m/s are selected for analysis. The statistical values of turbulence intensity at SCB site are shown in Table 1. The relationship between turbulence intensity and mean wind speed is shown in Fig. 7.

According to *Wind-resistant design specification for highway bridges* (Professional Standard PRC, 2004), the recommended I_u value of 0.11 was adopted for the SCB site, whereas the obtained I_u based on the full-scale wind data is obviously larger than the recommended value. This observation should be carefully considered in current and future bridge maintenance.

Table 1 Statistical values of turbulence intensity

	Mean	Standard Deviation
I_u	0.1406	0.0764
I_v	0.1234	0.0623
$I_u : I_v$	0.7478	

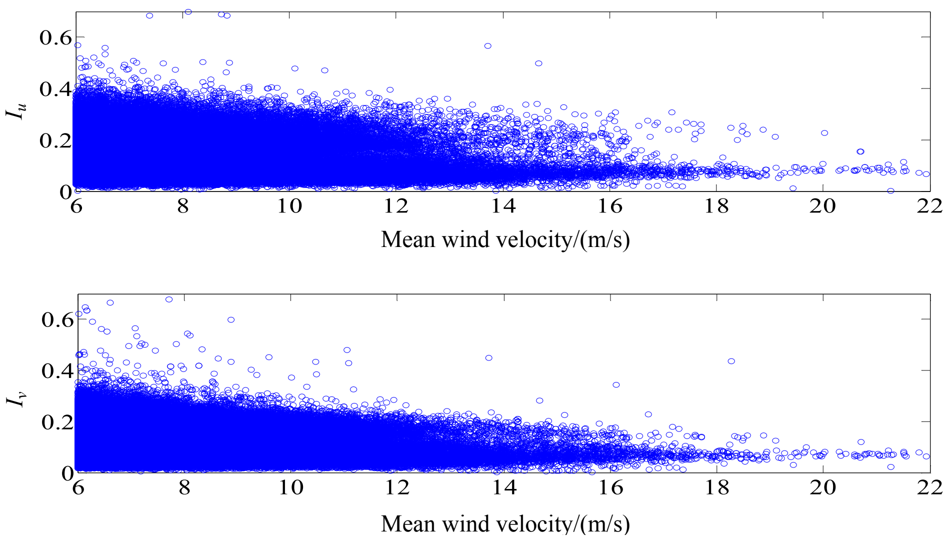

Fig. 7 Measured turbulence intensity on bridge deck with the mean wind speed larger than 6 m/s

As shown in Fig. 7, the measured I_u and I_v exhibit bifurcation as the wind speeds become larger. This phenomenon is observed probably because the wind data under investigation consists of the regular strong winds, typhoons and strong northern winds in winter. Turbulence intensity of the same mean wind speed varies among these winds governed by different generation mechanisms. For example, existing studies show that turbulence intensity is much larger during typhoons (Wang *et al*. 2013, Law *et al*. 2006). The difference of turbulence intensities between typhoons and strong northern winds in winter is yet to be analyzed.

Some researches show that there exists a linear relationship between I_u and I_v (Li *et al*. 2009). Based on long-term field measured data, the least square method is used to fit the data of I_u and I_v, as shown in Fig. 8.

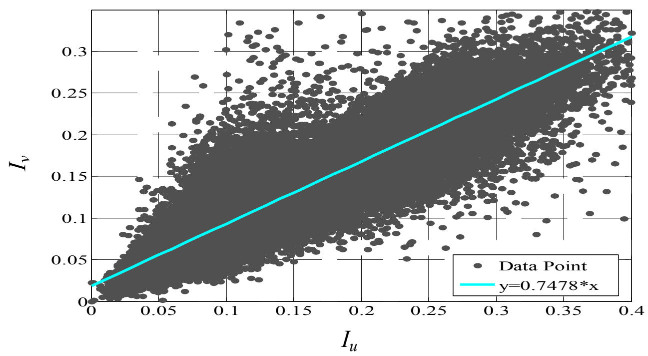

Fig. 8 Relationship between I_u and I_v on bridge deck

Fig. 8 shows $I_v/I_u \approx 0.7478$ after ignoring the sample with very low wind speed, which is lower than the reference value of 0.88 in *Wind-resistant design specification for highway bridges* (Professional Standard PRC, 2004). On the other hand, the obtained result of 0.7478 is higher than the recommended value of 0.5 by Solari and Piccardo (2001).

Sutong Bridge is under threat of typhoons annually due to its special geographical position. Typhoons often display non-stationary characteristics (Huang *et al.* 2015). Generally, non-stationary wind time history of typhoons at height *z* is usually expressed by the relationship (e.g., Chen and Letchford 2004, Su *et al.* 2015, Huang *et al*. 2015)

$$U(z,t) = \bar{U}(z,t) + \sigma(z,t)v'(z,t) \tag{3}$$

where $\bar{U}(z,t)$ represents deterministic time-varying mean wind speed; σ (z, t) is the slowly-varying deviation of turbulence; $v'(z, t)$ is referred to as the reduced turbulent fluctuation and usually follows the standard Gaussian distribution with zero mean and unit standard deviation (Chen and Letchford 2004).

Considering the physical meaning of turbulence intensity, Eq. (3) can be rewritten as

$$U(z,t) = \bar{U}(z,t)\left[1 + I_v(z,t)v'(z,t)\right] \tag{4}$$

where $I_t(z, t)$ is referred to as the time-varying turbulence intensity

$$I_t(z,t) = \frac{\sigma(z,t)}{\bar{U}(z,t)} \tag{5}$$

A variety of methods have been proposed to obtain the time-varying mean for non-stationary wind speeds (Bendat and Piersol 2000). In this study, the discrete wavelet transform (DWT) technique is adopted to derive the time-varying mean wind speed. In order to weak the dynamic magnification effects by the mean wind speed and capture the sudden variation trend of monitored data, the following empirical formula to determine the maximum frequency for time-varying mean wind speed at Sutong Bridge site is recommended as (Su *et al*. 2015)

$$\frac{1}{2t'} \le f_{\max} \le \frac{0.0637}{10} \tag{6}$$

where $f_{\max}$ represents the maximum frequency for time-varying mean wind speed; 0.0637 is the fundamental frequency of Sutong Bridge; t' denotes the pulse duration in wind record. As for typhoon, 150s is selected as the pulse duration in this study. Based on the Nyquist-Shannon theorem, $f_{\max}$ can be calculated by

$$f_{\max} = \frac{f_s}{2^{N+1}} \tag{7}$$

where f_s is sampling frequency; *N* represents the decomposition level. Based on the preceding discussions, *N*=7 seems to be a reasonable choice in this study. The following analyses adopt this decomposition level.

The slowly-varying deviation σ (z, t) is estimated using the Kernel Regression method in this study (e.g., Huang *et al*. 2015, Nadaraya 1964)

$$\sigma(z,t)=\sqrt{\frac{1}{K_b}\sum_{i=1}^{T}\left[U(z,t)-\bar{U}(z,t)\right]^2 K\left(\frac{t_i-t}{b}\right)} \tag{8}$$

where

$$K(t)=\frac{1}{\sqrt{2\pi}}\exp\left(-t^2/2\right) \tag{9}$$

and

$$K_b=\sum_{i=1}^{T}K\left(\frac{t_i-t}{b}\right) \tag{10}$$

where T is the total number of the monitored data, and b is the window.

Typhoon Fung-wong, Kalmaegi, Meari, Damrey, Haikui, Fitow, Trami, and Matmo are selected to be analyzed in this study. The data employed in the present work cover one hour, and what's more, the most intense wind speed occurs for t=1800 s. For the sake of brevity, Figs. 9 and 10 show the wind speed decomposition and time-varying turbulence intensity of typhoon Damrey and Meari, respectively. Panels (a)-(d) report, respectively, U with $\bar{U}$, σ, v' and I_t.

As shown in Figs. 9 and 10, it can be seen that the reduced turbulent fluctuation v' is almost totally lack of any trend when using N=7 as the decomposition level. It is obvious that σ captures slowly-varying trend in both of 'Damrey' and 'Meari'. As for typhoon Meari, I_t is generally a weakly-dependent function of time around 0.1.

However, as for typhoon Damrey, it is noted that I_t deviate from 0.1 for the time period of 2700-3600s due to the small time-varying mean wind speed. Table 2 shows the mean and standard deviation (Std) values of I_t for 8 typhoons in all.

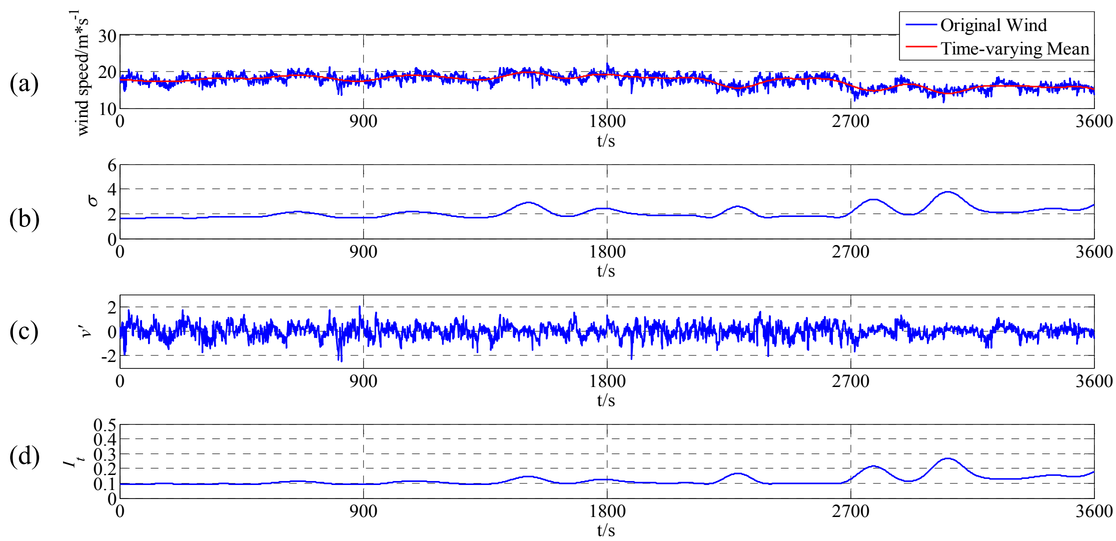

Fig. 9 Wind speed decomposition of Typhoon Damrey

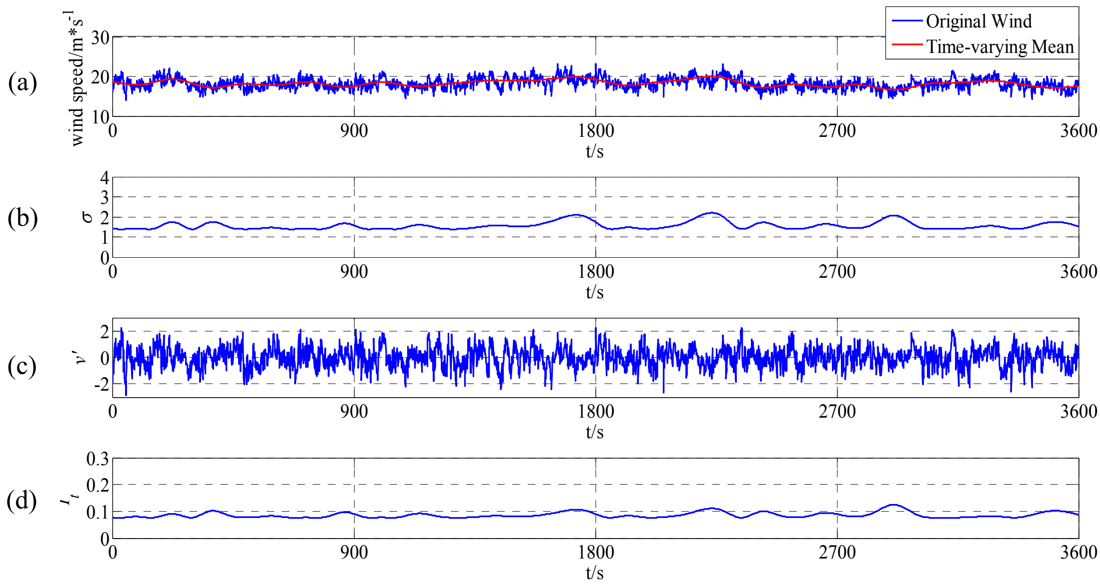

Fig. 10 Wind speed decomposition of Typhoon Meari

Table 2 Mean and Std values of I_t, for 8 typhoon records

Typhoon	Fung-wong	Kalmaegi	Meari	Damrey	Haikui	Fitow	Trami	Matmo
Mean(I_t)	0.2994	0.1529	0.0858	0.1210	0.1211	0.1449	0.0845	0.2529
Std(I_t)	0.1588	0.0414	0.0104	0.0347	0.0188	0.0202	0.0148	0.0660

Table 2 provides a comparison of the time-varying turbulence intensity among 8 typhoon events. It is worth noting that the mean values of I_t varies in the interval (0.08, 0.3) for aforementioned typhoons, while the Std values of I_t remain stable, very close to zero. It is noted that the mean values of I_t may be larger than those recommended (0.11) using stationary hypothesis. Referring to preceding phenomenon, several pioneers adopted the mean value of I_t to replace I_t during a suitable time interval. Such as I_t=0.25 (Chen and Letchford 2004), I_t=0.085-0.088 (Chen and Letchford 2007), I_t=0.01-0.25 (Chay *et al.* 2006). It is observed that whether and how much I_t can be regarded as a weakly-dependent function of time depends on the choice of time interval. The analysis of I_t for the monitored typhoons may provide useful information for this discussion. A non-dimensional function is introduced as following (Solari *et al.* 2015)

$$\eta(t) = \frac{I_t(t)}{\bar{I}_t} \tag{11}$$

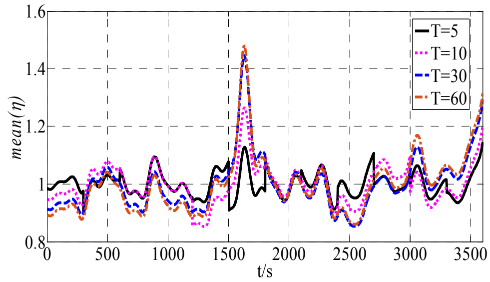

Fig. 11 Mean value of η with different time interval

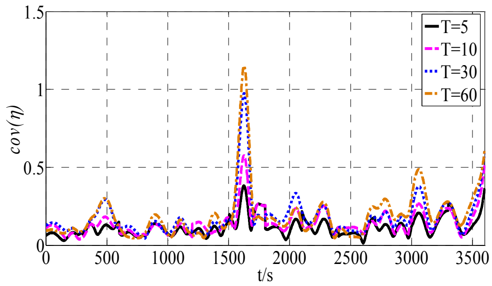

Fig. 12 Cov of η with different time interval

where $\overline{I}_t$ is the value of I_t averaged on a certain time interval T, T=5, 10, 30, 60 min, respectively. Fig. 11 shows the mean value of η as a function of time for all the typhoon records with T=5, 10, 30, 60 min, respectively. And Fig. 12 shows the cov of η as a function of time.

As shown in Figs. 11 and 12, it is worth noting that the mean value and cov of η are nearly independent of time with T=5min. As the T increasing, the mean value of η deviates further from 1, and the cov of η goes up at the same time. It follows that, for large level of T, using the average value of I_t to replace the time-varying I_t may not seems the best choice to describe the non-stationary wind speed model in Eq. (4). This matter deserves more studies with regard to the effect of the wind loading on structures.

4.2 Gust factor

Gust factor is another index that well reflects the intensity of fluctuation in natural winds (Beljaars 1987), which can be calculated by

$$G_u(t_g) = 1 + \frac{\max\left[\overline{u(t_g)}\right]}{U}, \quad G_v(t_g) = \frac{\max\left[\overline{v(t_g)}\right]}{U} \tag{12}$$

where U is mean wind speed; $\overline{u(t_g)}$ and $\overline{v(t_g)}$ are mean turbulence wind speed during t_g. The gust duration time t_g is commonly taken as 3s in structural wind engineering. Fig. 13 shows the probability distribution of the measured gust factor.

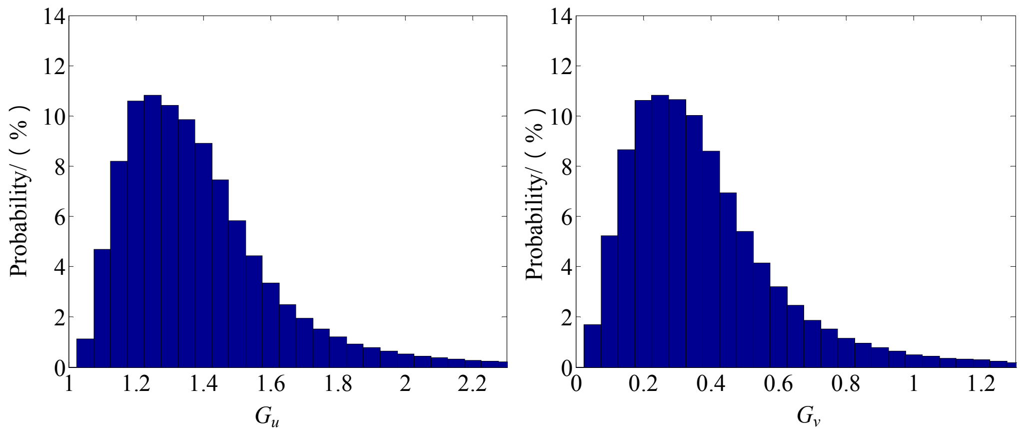

Fig. 13 Probability distribution of measured gust factor on bridge deck

As indicated in Fig. 13, most of the G_u are between 1.2 and 1.4 while G_v substantially ranges from 0.2 to 0.4. As mentioned above, only the data with mean wind speed larger than 6 m/s are adopted for analysis. The statistical values of the measured gust factor are listed in Table 3. The obtained gust factor G_u by Cao *et al*. (2015) is 1.397 based on the data with mean wind speed larger than 10 m/s during typhoons. It should be noted that the mean value of long-term measured G_u in Table 3 is probably lower than that calculated from the database covering a complete wind speed range (i.e., including very low wind speed).

Table 3 Statistical values of gust factor

	Mean Value	Standard deviation
G_u	1.2720	0.1270
G_v	0.2709	0.1327

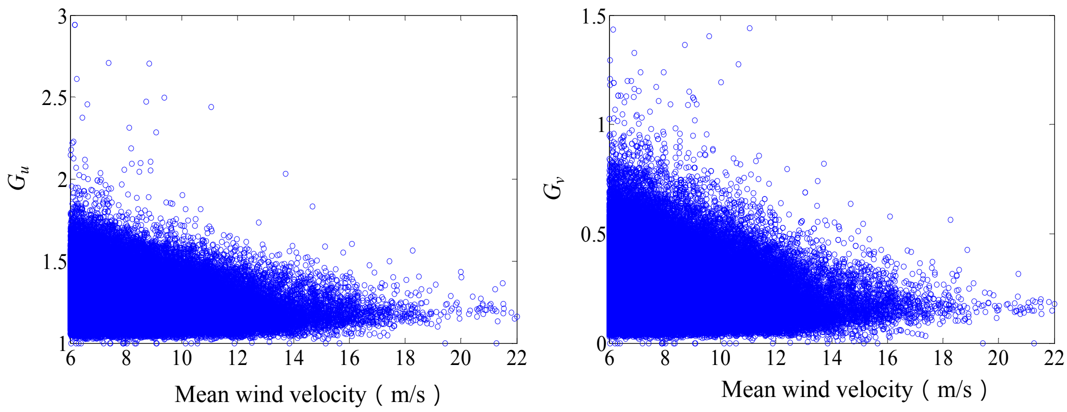

Fig. 14 Measured gust factor VS. Mean wind speed

Fig. 14 shows the measured gust factor with the mean wind speed. It indicates the gust factor tends to converge as the mean wind speed increases. The parameter fitting studies between I_u and G_u based on the measured data have been developed (Cao *et al*. 2009, Ishizaki 1983, Choi 1983).

The fitting equation of I_u with G_u can be constructed as

$$G_u = 1 + k_1 \times I_u^{k_2} \ln(\mathrm{T}/\mathrm{t}_g) \tag{13}$$

where T is basic interval; t_g is the gust duration time. The fitting parameters k_1=0.5 and k_2=1.0 are suggested by Ishizaki (1983), and k_1=0.62 and k_2=1.27 are suggested by Choi (1983). The relationship between gust factor and turbulence intensity is also not linear in the study of Cao et al. (2015).

Fig. 15 shows the relationship between gust factor and turbulence intensity based on the wind data of SHMS on SCB. With the basic interval of 10min and gust duration time of 3s, it can be calculated that the fitting parameters k_1 and k_2 are 0.3982 and 1.02 based on the long-term measured data, respectively. The obtained relationship between I_u and G_u is almost linear, as suggested by Ishizaki (1983). On the other hand, the obtained slope k_1 in this study is smaller than those in both Ishzaki and Choi models, as shown in Fig. 15. This suggests that the obtained G_u is relatively smaller. Although a linear relationship is fitted, it should be noted that the significantly scattered measurements are observed in the figure, especially at high values of I_u and G_u.

4.3 Turbulence integral length scale

The spatial correlation could be estimated using a temporal correlation function based on the Taylor hypothesis. As a result, the turbulence integral length scale is usually calculated by the auto-correlation function integral method

$$L_u^x = \frac{U}{\sigma_u^2} \int_0^\infty R_u(\tau)\,\mathrm{d}\tau \tag{14}$$

where $R_u(\tau)$ is the auto-correlation function. Since the errors caused by Taylor hypothesis would increase with a small value of $R_u(\tau)$, an integral upper limit should be selected. In this study, the upper limit is taken as the value of $R_u(\tau) = 0.05\sigma_u^2$ (Wang *et al*. 2010).

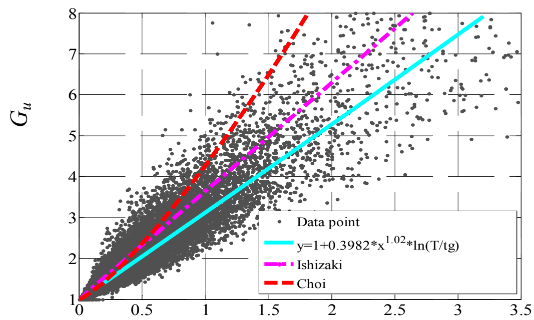

Fig. 15 Gust factor VS. Turbulence intensity on bridge deck

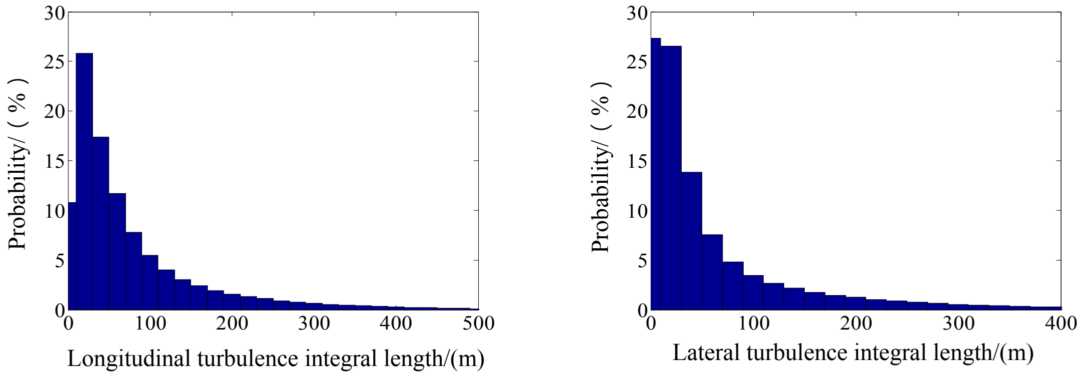

Fig. 16 Probability distribution of turbulence integral length scale on bridge-deck level

Fig. 16 shows the statistical distribution of measured longitudinal and lateral 10-min turbulence integral length scale. It is noted that most of the longitudinal turbulence integral length scales on the bridge-deck level are between 40 and 100 m, while the lateral value ranges from 0 to 80 m. The statistical mean value of longitudinal integral length scale of typhoon recoded by the SHMS on Sutong Bridge is 156.83 and the lateral scale is 98.84. The longitudinal integral length scale is smaller than the measured value during typhoons ($L_u^x = 271.7, L_v^x = 98.7$) by Hui *et al*. (2009), while the lateral integral length scale is close.

4.4 Turbulence power spectra

The hourly turbulence wind data of Typhoon Damrey from 15:00 to 16:00 on Aug. 1 (U=7.397 m/s), from 16:00 to 17:00 on Aug. 1 (U=9.072 m/s), from 05:00 to 06:00 on Aug. 3 (U=10.613 m/s), from 08:00 to 09:00 on Aug. 3 (U=14.311 m/s), from 09:00 to 10:00 on Aug. 3 (U=16.379 m/s) and from 14:00 to 15:00 on Aug. 3 (U=17.342 m/s), in 2012 have been respectively selected to calculate the turbulence power spectra. The measured spectra are compared with the commonly adopted PSDs (Karman, Kaimal, Davenport, Simiu), whose parameters are taken from the *Chinese Wind-Resistant Design Specification for Highway Bridges* (Professional Standard PRC, 2004).

These spectra are detailed as below (Soyoz and Feng 2009, Hu *et al*. 2010, Wang *et al*. 2013):

Karman spectra

$$\frac{\mathrm{n}S_u(\mathrm{Z},\mathrm{n})}{\left(u^*\right)^2} = \frac{4\beta f}{\left(1+70.8 f^2\right)^{5/6}} \tag{15}$$

$$f = nL_u^x / U \tag{16}$$

$$\sigma_u^2 = \beta\left(u^*\right)^2 \tag{17}$$

Kaimal spectra

$$\frac{nS_u(Z,n)}{(u^*)^2} = \frac{200f}{(1+50f)^{5/3}} \tag{18}$$

$$f = \frac{nZ}{U} \tag{19}$$

Davenport spectra

$$\frac{nS_u(Z,n)}{(u^*)^2} = \frac{4f^2}{(1+f^2)^{4/3}} \tag{20}$$

$$f = \frac{nL_u}{U(10)} \tag{21}$$

Simiu spectra

$$\frac{nS_u(Z,n)}{\sigma_u^2} = \frac{200f}{6\left(1+50f^2\right)^{5/3}} \tag{22}$$

$$f = \frac{nZ}{U} \tag{23}$$

where S_u is the auto-power spectral density of longitudinal turbulence; Z represents the altitude of the wind speed relative to the sea level; $U(10)$ is the mean wind speed at the height of 10 m; $u*$ is the friction wind speed; f is the Moning Coordinate; β is the coefficient of friction wind speed; σ_u is the standard deviation of longitudinal turbulence. The energy normalization method $\sigma_u^2 = 6(u^*)^2$ is used in the calculation of Simiu spectra.

The abovementioned spectra are shown in Fig. 17, which reveals that the measured spectra generally matches well with the Kaimal and Karman spectra in low-frequency regions for the longitudinal turbulence, while Davenport and Kaimal spectra present relatively better agreement with the measured spectra in high-frequency region. In general, it is concluded that the Kaimal spectra can be recommended for the SCB site (Wang 2010).

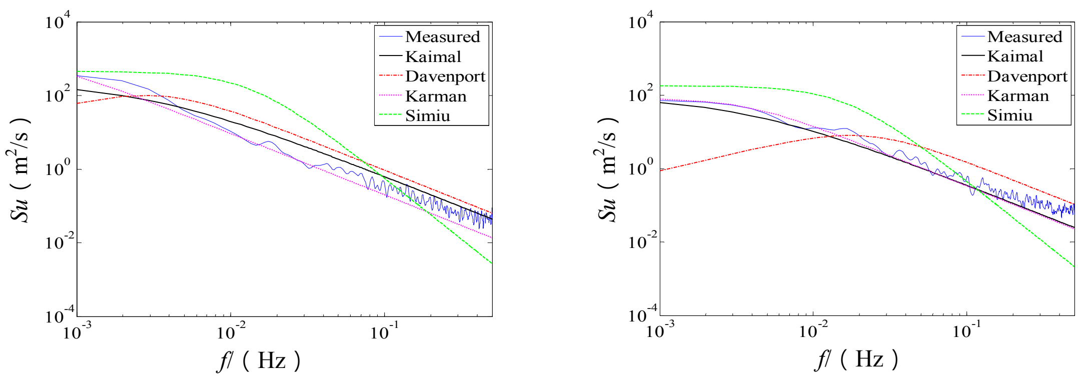

(a) Mean wind speed of 7.397 m/s (b) Mean wind speed of 9.072 m/s

Continued-

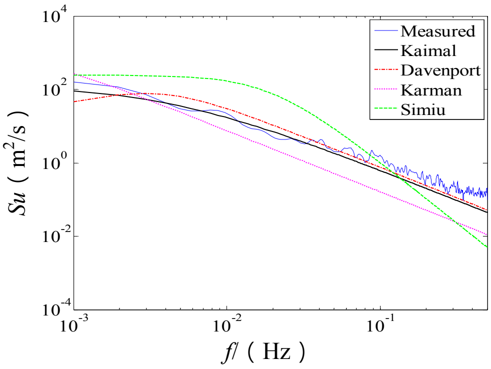

(c) Mean wind speed of 10.613 m/s

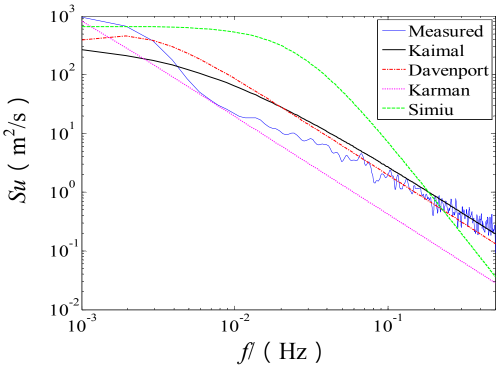

(d) Mean wind speed of 14.311 m/s

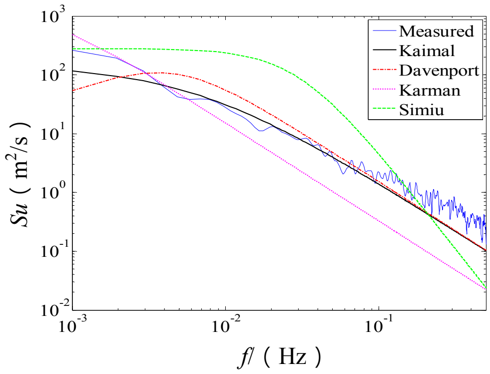

(e) Mean wind speed of 16.379 m/s

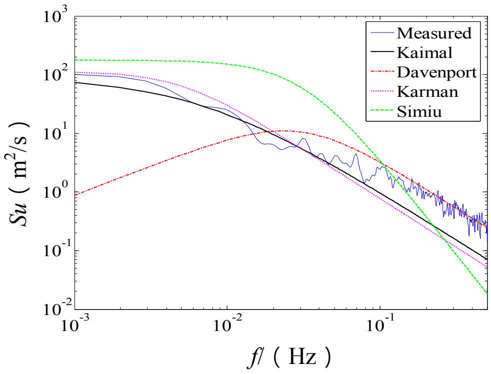

(f) Mean wind speed of 17.342 m/s

Fig. 17 Comparison of longitudinal power spectra under various wind speeds

5. Conclusions

In this study, based on the statistical analysis of the long-term monitoring wind data from the SHMS of Sutong Bridge, the following concluding remarks can be made:

- From Jan. 1, 2008 to Mar. 31, 2015, the maximum 10-min mean wind speed on the bridge deck of SCB is 23.42 m/s, while the average wind speed is 5.31 m/s. The long-term monitoring 10-min mean wind speed verifies the reliability of the recommended values in the current specification of China. Meanwhile, the wind rose diagram shows that the dominant southeast wind is in accordance with the climate environment at SCB site.
- The statistical results of longitudinal turbulence intensity for the mean wind speed over 6 m/s reveal the measured value (i.e., 0.14) is slightly larger than the code specified one (i.e., 0.11), while I_v/I_u ratio (i.e., 0.75) is smaller than the code one (i.e., 0.88). These discrepancies should be carefully considered during bridge maintenance and for new bridge designs around this region.
- The reduced turbulent fluctuation *v'* is almost totally lack of any trend when using N=7 as the decomposition level. The mean values of I_t varies in the interval (0.08, 0.3) for typhoons analyzed

in this study, while the Std values of I_t remain stable, very close to zero. It is noted that the mean values of I_t may be larger than those recommended (0.11) using stationary hypothesis. As for large level of time interval, using the average value of I_t to replace the time-varying I_t may not seems the best choice to describe the non-stationary wind speed model in Eq. (4). This matter deserves more studies.

- The nonlinear fitting results of measured turbulence intensity with gust factor show that the parameter k_2 is close to the recommended data (i.e., 1.0) by Ishizaki, which indicates an approximately linear relationship at the SCB site.
- The 10-min longitudinal turbulence integral length scale for the SCB concentrates between 40 m and 100 m, while the substantial lateral values range from 0m to 80 m. The statistical mean value of turbulence integral length scale is smaller than the value during typical typhoons.
- The measured longitudinal wind power spectra agree well with the Kaimal and Karman spectra in the low-frequency region, while Davenport and Kaimal spectra match well with measured spectra in high-frequency region. In general, Kaimal spectra is recommended for the SCB site.

Acknowledgements

The supports of the Major State Basic Research Development Program (973 Program) of China (No. 2015CB060000), the National Science Foundation of China (Nos. 51378111 and 51438002), and the Fok YingTong Education Foundation for Young Teachers in the Higher Education Institutions of China (No. 142007) are greatly acknowledged.

References

Andersen, O.J. and Lovseth, J. (1995), "Gale force maritime wind, the Froya database. Part 1: sites and instrumentation, review of the database", *J. Wind Eng. Ind. Aerod.*, **57**(1), 97-109.

Beljaars, A.C.M. (1987), "The influence of sampling and filtering on measured wind gusts", *Am. Meteorol. Soc.*, **4**(4), 613-626.

Bendat, J.S. and Piersol, A.G. (2000), *Random data: Analysis and measurement procedures*, Wiley, New York.

Cao, S.Y., Tamura, Y., Kikuchi, N., Saito, M., Nakayama, I. and Matsuzaki, Y. (2009), "Wind characteristics of a strong typhoon", *J. Wind Eng. Ind. Aerod.*. **97**(1), 11-21.

Cao, S.Y., Yukio, T., Naoshi, K., *et al.* (2015), "A case study of gust factor of a strong typhoon", *J. Wind Eng. Ind. Aerod.*, **138**, 52-60.

Chay, M.T., Albermani, F. and Wilson, B. (2006), "Numerical and analytical simulation of downburst wind loads", *Eng. Struct.*, **28**(2), 240-254.

Chen, L. and Letchford, C.W. (2004), "A deterministic-stochastic hybrid model of downbursts and its impact on a cantilevered structure", *Eng. Struct.*, **26**(5), 619-629.

Chen, L. and Letchford, C.W. (2007), "Numerical simulation of extreme winds from thunderstorm downbursts", *J. Wind Eng. Ind. Aerod.*, **95**, 977-990.

Choi, E.C.C. (1983), *Wind loading in Hong Kong: commentary on the Code of Practice on Wind Effects Hong Kong-1983*, Hong Kong: Hong Kong Institution of Engineers.

Deaves, D.M. and Harris, R.I. (1978), "A mathematical mode of the structure of strong winds", *CIRIA*

Report, (76), 23-29.
Deng, Y., Liu, Y., Feng, D.M. and Li, A.Q. (2015), "Investigation of fatigue performance of welded details in long-span steel bridges using long-term monitoring strain data", *Struct. Control Health Monit.*, **22**(11), 1343-1358.
Flay, R.G.J. and Stevenson, D.C. (1998), "Integral length scales in strong winds below 20 m", *J. Wind Eng. Ind. Aerod.*, **28**(1-3), 21-30.
Fu, J.Y., Li, Q.S., Wu, J.R., Xiao, Y.Q. and Song, L.L. (2008), "Field measurements of boundary layer wind characteristics and wind-induced responses of super-tall buildings", *J. Wind Eng. Ind. Aerod.*, **96**(8-9), 1332-1358.
Hu, R.M., Wang, H. and Li, A.Q. (2010), "Measurement study on wind characteristics of Typhoon Kalmaegi on the Sutong Bridge", *Wuhan Univ. J. Natural Sci.*, **15**(2), 153-159.
Huang, G.Q., Peng, L.L., Su, Y.W., Liao, H. and Li, M. (2015), "A wireless high-frequency anemometer instrumentation system in field measurement", *Wind Struct.*, **20**(6), 739-749.
Huang, G.Q., Zheng, H.T., Xu, Y.L. and Li, Y.G. (2015), "Spectrum models for nonstationary extreme winds", *J. Struct. Eng. - ASCE*, **141**(10).
Hui, M.C., Larsen, A. and Xiang, H.F. (2009a), "Wind turbulence characteristics study at the Stonecutters Bridge site: part Ⅰ- mean wind and turbulence intensities", *J. Wind Eng. Ind. Aerod.*, **97**(1), 22-36.
Hui, M.C., Larsen, A. and Xiang, H.F. (2009b), "Wind turbulence characteristics study at the Stonecutters Bridge site: part ⅠⅠ-wind power spectra, integral length scales and coherences", *J. Wind Eng. Ind. Aerod.*, **97**(1), 48-59.
Ishizaki, H. (1983), "Wind profiles, Turbulence intensities and gust factors for design in typhoon-prone regions", *J. Wind Eng. Ind. Aerod.*, **13**(1-3), 55-66.
Law, S.S., Bu, J.Q. and Zhu, X.Q. (2006), "Wind characteristics of Typhoon Dujuan as measured at a 50 m guyed mast", *Wind Struct.*, **9**(5), 387-396.
Li, L.X., Kareem, A.S., Xiao, Y.Q., Song, L.L. and Zhou, C.Y. (2015), "A comparative study of field measurements of the turbulence characteristics of typhoon and hurricane winds", *J. Wind Eng. Ind. Aerod.*, **140**, 49-66.
Li, L.X., Xiao, Y.Q., A.K., Kareem, A.S., Song, L.L and Qin, P. (2012), "Modeling typhoon wind power spectra near sea surface based on measurements in the South China sea", *J. Wind Eng. Ind. Aerod.*, **104-106**, 565-576.
Li, Q.S., Zhi, L.H. and Hu, F. (2009), "Field monitoring of boundary layer wind characteristics in urban area", *Wind Struct.*, **12**(6), 553-574.
Ministry of Transport of the People's Republic of China, (2004), *Wind-resistant design specification for highway bridges*, Beijing, China Communications Press.
Miyata, T., Yamada, H., Katsuchi, H. and Kitagawa, M. (2002), "Full-scale measurements of Akashi-Kaikyo Bridge during typhoon", *J. Wind Eng. Ind. Aerod.*, **90**(12-15), 1517-1527.
Nadaraya, E.A. (1964), "On estimating regression", *Theory Probab. & Its Appl.*, **9**(1), 141-142.
Pang, J.B., Lin, Z.X. and Ge, Y.J. (2002), "Field measurements of strong wind characteristics in Pudong district", *Exp. Meas. Fluid Mech.*, **16**(3), 32-39.
Sharma, R.N. and Richards, P.J. (1999), "A re-examination of the characteristics of tropical cyclone winds", *J. Wind Eng. Ind. Aerod.*, **83**(1-3), 21-33.
Shu, Z.R., Li, Q.S., He, Y.C. and Chan, P.W. (2015), "Gust factors for tropical cyclone, monsoon and thunderstorm winds", *J. Wind Eng. Ind. Aerod.*, **142**, 1-14.
Solari, G., Burlando M., De Gaetano P., *et al*. (2015), "Characteristics of thunderstorms relevant to the wind loading of structures", *Wind Struct.*, **20**(6), 763-791.
Solari, G. and Piccardo, G. (2001), "Probabilistic 3-D turbulence modeling for gust buffeting of structures", *Probabilist. Eng. Mech.*, **16**(1), 73-86.
Soyoz, S. and Feng, M.Q. (2009), "Long-term monitoring and identification of bridge structural parameters", *Comput. -Aided Civil Infrastruct. Eng.*, **24**(2), 82-92.
Sparks, P.R., Reid, G.T., Reid, E.D., Welsh, S. and Weish, N. (1992), "Wind conditions in hurricane Hugo

by measurement, inference and experience", *J. Wind Eng. Ind. Aerod.*, **41**(1-3), 55-66.
Su, Y.W., Huang, G.Q. and Xu, Y.L. (2015), "Derivation of time-varying mean for non-stationary downburst winds", *J. Wind Eng. Ind. Aerod.*, **141**, 39-48.
Toriumi, R., Katsuchi, H. and Furuya, N. (2000), "A study on spatial correlation of natural wind", *J. Wind Eng. Ind. Aerod.*, **87**(2-3), 203-216.
Wang, H., Li, A.Q., Niu, J., Zong, Z.H. and Li, J. *(*2013), "Long-term monitoring of wind characteristics at Sutong Bridge site", *J. Wind Eng. Ind. Aerod.*, **115**, 39-47.
Wang, H., Li, A.Q., Jiao, C.K. and Li, X.P. (2010), "The characteristics of strong winds at the Runyang Suspension Bridge based on field tests from 2005 to 2008", *J. Zhejiang Univ. Sci. A (Applied Physics & Engineering)*, **11**(7), 465-476.
Wang, H., Tao, T.Y. and Wu, T. (2016), "Wind power spectra for coastal area of East Jiangsu Province based on SHMS", *Wind Struct.*, **22**(2), 235-252.
Wills, J.A.B., Grant, A. and Boyack, C.F. (1986), *Offshore mean wind profile*, *Department of Energy*, Offshore Technical Report, OTH86266.
Xiao, Y.Q., Li, L.X. and Song, L.L. (2010), "Study on typhoon wind characteristics based on seashore measurements", *Proceedings of the 11th international symposium on structural engineering*.
Xu, Y.L., Zhu, L.D. and Wong, K.Y. (2000), "Field measurement results of Tsing Ma suspension bridge during Typhoon Victor", *Struct. Eng. Mech.*, **10**(6), 545-559.
You, Q.Z., He, P., Dong, X.W., Zhang, X. and Wu, S.C. (2008), "Sutong Bridge - The longest cable-stayed bridge in the world", *J. Int. Assoc. Bridge Struct.Eng.*, **18**(4), 390-395.
Zhang, X.G. and Chen, A.R. (2010), "Sutong Bridge design and structural performance", *China Communications Press*, 36-37.

CC